The micromechanical signature of pituitary adenomas: new perspectives for the diagnosis and surgery

Mikaël Meyer, Nicolas Bouchonville, Christophe Gaude, Emmanuel Gay, David Ratel, Alice Nicolas

▶ **To cite this version:**

Mikaël Meyer, Nicolas Bouchonville, Christophe Gaude, Emmanuel Gay, David Ratel, et al.. The micromechanical signature of pituitary adenomas: new perspectives for the diagnosis and surgery. Advanced NanoBiomed Research, 2021, 1 (9), pp.2000085. 10.1002/anbr.202000085 . hal-03363563

HAL Id: hal-03363563

https://hal.archives-ouvertes.fr/hal-03363563

Submitted on 5 Oct 2021

HAL is a multi-disciplinary open access archive for the deposit and dissemination of scientific research documents, whether they are published or not. The documents may come from teaching and research institutions in France or abroad, or from public or private research centers.

L'archive ouverte pluridisciplinaire **HAL**, est destinée au dépôt et à la diffusion de documents scientifiques de niveau recherche, publiés ou non, émanant des établissements d'enseignement et de recherche français ou étrangers, des laboratoires publics ou privés.

ADVANCED NANOBIOMED RESEARCH
www.advnanobiomedres.com

The Micromechanical Signature of Pituitary Adenomas: New Perspectives for the Diagnosis and Surgery

Mikaël Meyer, Nicolas Bouchonville, Christophe Gaude, Emmanuel Gay, David Ratel, and Alice Nicolas**

Pituitary adenomas are common tumors in the skull base that are associated with significant morbidity due to local compressive effects, hormonal hypersecretion, or treatment-associated endocrine deficiency. Pituitary adenomas are often surgically resected to improve clinical symptoms, with the help of magnetic resonance imaging (MRI) to locate the tumor tissues. But still a large proportion of adenoma fail being located, being either too small or not dense enough. In addition, normal and tumor tissues do not always show optical contrast in endoscopic endonasal trans-sphenoidal surgery. Finding new markers to delineate the tumor tissue has become mandatory to help the surgical procedure and limit relapses. Herein, an indentation-type atomic force microscope is used to show that tumor tissues are two orders of magnitude softer than normal tissues, independent of the type of hormonal secretion. This softening correlates with the degradation of the reticulin, type IV collagen, and laminin scaffolds in all the tumors. This significant difference suggests that intraoperative lesion localization and margin assessment could be evaluated by an approach based on stiffness measurement.

1. Introduction

More and more studies report on differences of the mechanical properties of healthy and tumor tissues in human. Breast tumor tissues for instance are stiffer than normal ones,[1,2] and this difference in stiffness is used as a medical prognostic of a mammary tumor. Stiffening of the tumor tissue was also observed for other cancers such as pancreatic ductal adenocarcinoma,[3] or some brain cancers (meningioma or glioma[4] and glioblastoma[5]). Alteration of the mechanical properties of the tumor tissues was shown to originate from change in rigidity of both the cells and the extracellular matrix (ECM).[6] Independent of the biological and physical mechanisms at the origin of this alteration,[7] this suggests that the stiffness mismatch between normal and tumor tissues could be used as a marker to delineate tumor tissues, similar to what is done with biological markers.

Here, we focus on pituitary adenomas. Pituitary adenoma represents the most common tumor in the sellar region.[8] The incidence of these intracranial tumors is ranking third, accounting for 15% among all primary intracranial neoplasms.[9] Pituitary adenomas are often surgically resected to improve the clinical symptoms. Endoscopic endonasal trans-sphenoidal surgery is a common treatment for these patients. The surgical act is based on the visualization of the tumor contour by MRI. Many tumors however keep invisible, due to the limited resolution of MRI and the lack of useful sequences.[10] Then delineating the tumor in this organ is challenging, and incomplete or excessive resection leads either to tumor recurrence or life-long alteration of the patient's life with hormonal disorders.

Following results obtained on other organs, we investigate here whether human pituitary adenoma show significantly different mechanical properties compared with the normal tissue. The aim is to conclude on the feasibility of using the mechanical properties of the pituitary tissue, and more specifically its elastic properties, as a marker of adenoma and use it to help the surgical act. We use indentation-type atomic force microscopy (IT-AFM) to characterize the elastic properties of pituitary adenomas from six patients. The choice of this technique comes from the small size of the tumors, of 1 mm or less. Similar to most biological tissues, pituitary tissues only show linear elastic behavior on a

Dr. M. Meyer, Prof. E. Gay
Neurosurgery Department
CHU Grenoble Alpes
F-38000 Grenoble, France

Dr. N. Bouchonville, Dr. A. Nicolas
CNRS, LTM
Université Grenoble Alpes
F-38000 Grenoble, France
E-mail: alice.nicolas@cea.fr

C. Gaude, Dr. D. Ratel
CEA, LETI
Clinatec
Université Grenoble Alpes
F-38000 Grenoble, France
E-mail: david.ratel@cea.fr

The ORCID identification number(s) for the author(s) of this article can be found under https://doi.org/10.1002/anbr.202000085.

© 2021 The Authors. Advanced NanoBiomed Research published by Wiley-VCH GmbH. This is an open access article under the terms of the Creative Commons Attribution License, which permits use, distribution and reproduction in any medium, provided the original work is properly cited.

DOI: 10.1002/anbr.202000085

limited range of deformation and have strong adhesive interaction with the AFM probe. Here, we account for these limitations following a methodology we have formerly implemented.[11,12] As a result, we show that human pituitary adenomas are significantly softer than the healthy tissue, and that this softening is associated to the degradation of reticulin, laminin, and collagen IV scaffolds.

2. Results

2.1. Micromechanical Signatures of Normal and Tumor Human Pituitary Tissues

To investigate the mechanical properties of human pituitary adenoma, eight human specimen (two healthy pituitary tissues and six pituitary adenoma, **Table 1**) were obtained from surgery and were studied using IT-AFM in phosphate buffer saline (PBS). The experimental approach for obtaining stiffness distribution across entire tissue fragments is described in **Figure 1**a. To confirm the tumor state of the tissue, a histological staining (hematoxylin and eosin [HE]) of the sections dedicated to the indentation experiment was conducted on a mirror section. With the exception of a specimen that showed mixed tumor and normal histological patterns within few sections, all the other sections were of uniform histological subtype. We could therefore relate randomly distributed indentation maps to histological subtypes. We first compared the mechanical properties of healthy and adenoma sections, with no distinction of the adenoma subtype. To this end, we carried out IT-AFM using a micrometer-sized indenter, of 10 μm diameter. This ensured a μm^2 contact area between the AFM probe and the sample. The measured stiffness was therefore averaged at the micrometer scale, which is also the scale of a well-documented rigidity-sensitive adhesion machinery of cells named focal adhesions.

We observed that both category (healthy and tumor tissues) shows a unimodal stiffness distribution, but that the median stiffness of the both differs of two orders of magnitude (Figure 1). Healthy tissues showed a median stiffness of 9.7 kPa, with 66% of the values around the median being comprised between 3.7 and 27.0 kPa (Figure 1b, left). The adenoma tissues showed a median stiffness of 0.12 kPa (66% values interval: 0.04–0.38 kPa) (Figure 1c, left). The difference between healthy and tumor tissues was significant (Welch's *t*-test, $p = 0.0009$) (Figure 1d). It is to be noted that in the range of the indentation velocities we tested, we did not observe any drift in the measured Young's moduli, thus showing that both healthy[11] and tumor tissues were not noticeably viscous in this range of velocity (Figure S1, Supporting Information). Comparison of HE-stained sections revealed that healthy tissues contain nested cells surrounded by a rich capillary network (Figure 1b, right), while adrenocorticotrophic hormone (ACTH)-secreting microadenoma showed a very characteristic dense Crooke cells content and the absence of capillary network (Figure 1c, right). We thus hypothesized that the dramatic softening of the tumor tissue could be caused by a modification of the cell content and by dramatic changes in the organization of the extracellular matrix.

2.2. Changes in Micromechanical Properties in Pituitary Adenomatous Tissue Correlates with Matrix Degradation

To correlate the respective micromechanical profiles to pathohistological findings in normal and adenomatous pituitary fragments, staining of ex vivo pituitary fragments under physiological buffer conditions was carried out. We investigated the composition and distribution of the ECM in the normal and adenomatous pituitary fragments and correlated it to the loss of rigidity (**Figure 2**). Normal pituitary tissue sections revealed a highly heterogeneous stiffness, with gradients of the order of several kPa μm^{-1} (Figure 2a–c) as already reported.[11] This was associated with a dense network of reticulin, a fiber of the ECM abundantly present in normal pituitary tissues (Figure 2d). Collagen IV and laminin were also organized in a dense ECM network (Figure 2e–f). Adenomatous pituitary sections revealed a much softer and more uniform stiffness, with stiffness gradients a hundred times smaller than on healthy tissues (Figure 2g–i, Figure S2, Supporting Information). Ex vivo tissue labeling revealed a decrease in the level of reticulin content

Table 1. Clinical summary of patients and stiffness of the specimens used in this study. ACTH: adrenocorticotropic hormone; PL: prolactin; GH: growth hormone; FSH: follicle-stimulating hormone; LH: luteinizing hormone; NA: not applicable. Median values of the Young's moduli are obtained with models that consider the adhesion of the AFM probe with the tissue (JKR's model) or neglect it (Hertz's model). Values in parenthesis are the low and high boundaries that enclose 66% of the values.

Specimen	Age, y/sex	Diagnosis	Hormone	No force curves	E_{JKR} [kPa]	E_{Hertz} [kPa]
1	46/F	Adenoma	ACTH	174	0.17 (0.08, 0.44)	0.28 (0.12, 0.65)
2	46/F	No lesion	NA	953	14.12 (5.45, 41.89)	38.45 (7.08, 54.02)
3	48/M	Adenoma	ACTH	471	0.08 (0.02, 0.25)	0.11 (0.03, 0.34)
4	40/F	Adenoma	GH, PL	301	0.19 (0.08, 0.62)	0.26 (0.10, 0.77)
5	29/F	Adenoma	GH	458	0.09 (0.03, 0.22)	0.20 (0.07, 0.45)
6	49/M	Adenoma	FSH	292	0.29 (0.10, 0.51)	0.37 (0.12, 0.66)
7	86/M	Adenoma	LH	266	0.05 (0.03, 0.12)	0.07 (0.04, 0.17)
8	46/F	No lesion	NA	819	7.02 (2.49, 13.46)	10.84 (4.10, 20.95)
8	46/F	Adenoma	ACTH	100	0.41 (0.08, 2.04)	0.73 (0.10, 5.88)

© 2021 The Authors. Advanced NanoBiomed Research published by Wiley-VCH GmbH

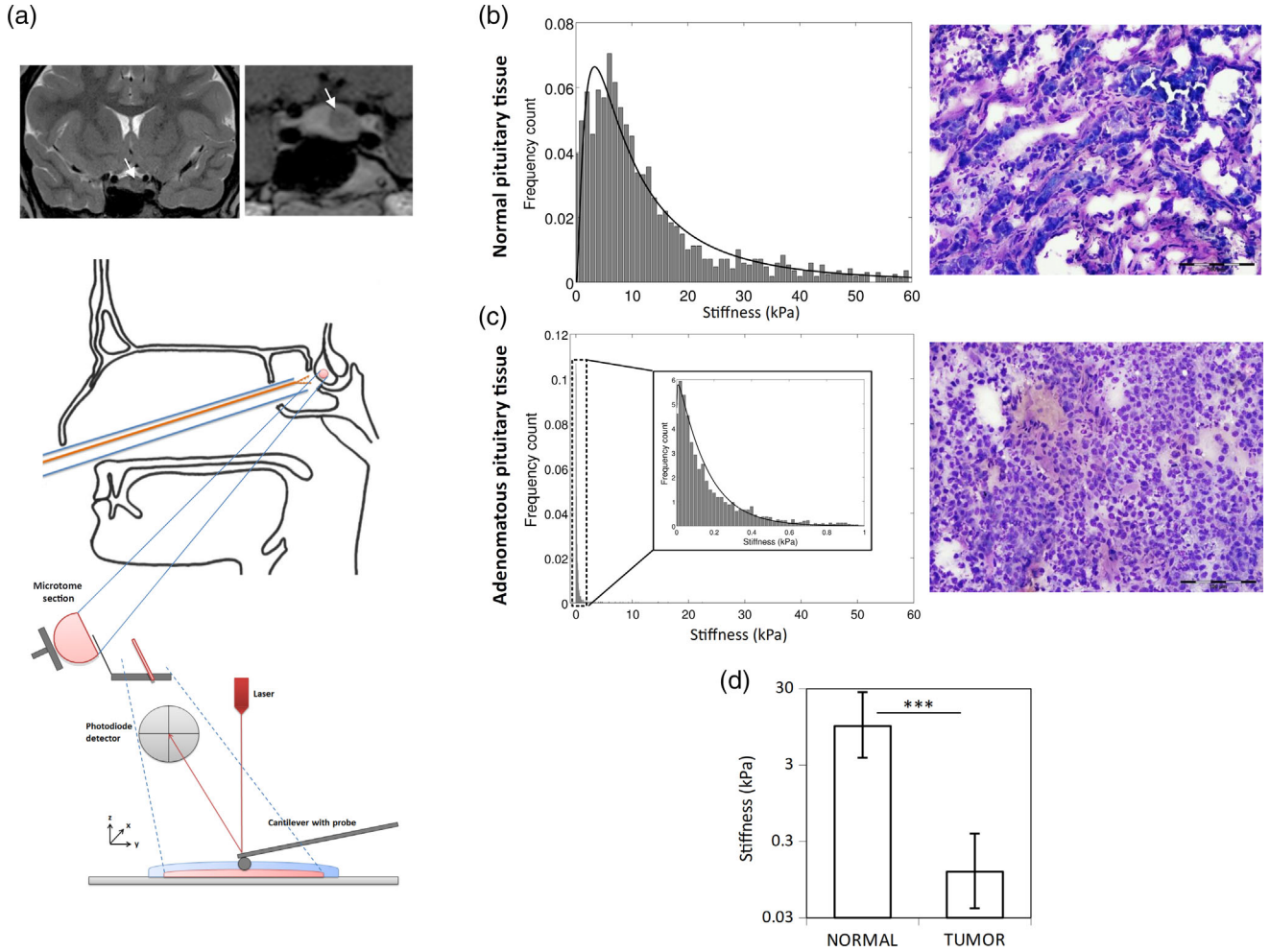

Figure 1. Micromechanical signature of human pituitary tissue. a) Top left: coronal contrast-enhanced magnetic resonance imaging demonstrated the mass lesion of ACTH-secreting pituitary adenoma. Top right: zoom on the mass lesion. Bottom: schematic of an endonasal endoscopic trans-sphenoidal pituitary surgery from a patient with a suspicious mass lesion, microtome section of the mass lesion and transversal view of a glass slide-immobilized adenoma section in PBS with the cantilever (with spherical probe) positioned for IT-AFM. b) Left: stiffness distribution for normal pituitary gland tissue based on 11 randomly selected areas ($90 \times 90\,\mu m^2$) in two specimens. Histogram reveals a unimodal and a broad stiffness distribution. Inset: representative retract force–indentation curve (black line) fitted with JKR elastoadhesive model (red dashed line, 3.91 kPa) within the elastic linear region (in between the dotted lines). Right: post-AFM histology reveals normal pituitary gland tissue recognized by its specific architectural pattern composed of nested cells surrounded by a rich capillary network. Scale bar: 100 µm. c) Left: stiffness distribution for adenomas is narrower with a significantly reduced stiffness compared to normal pituitary gland tissue (24 randomly distributed maps of seven specimens). Inset as in (b) (Young's modulus 0.09 kPa). Right: post-AFM histology shows a different morphology compared with normal tissue. ACTH-secreting adenoma shows adenoma Crooke cells characterized by densely eosinophilic and hyaline cytoplasm. d) Pituitary adenomas are statistically much softer than normal tissues (respectively, 0.1 and 9.7 kPa, $p < 0.001$). Bars show the 66% percentiles around the median.

as expected for adenomatous tissues, as well as of collagen IV and laminin (Figure 2j–l).

Reticulin fibers are an important component of the network structure of ECM in the pituitary gland. They play a major role in maintaining the elasticity of the organ. We could therefore relate the decrease in the expression of the reticulin fibers to the loss of rigidity observed in the adenomatous pituitary. In addition, in normal pituitary tissue, collagen IV, the main constituent of the basal lamina, has a regular structure forming a well-organized dense network (Figure 2e). In our study, we observed that collagen IV level in the adenomatous tissue is sorely decreased and loses its network organization (Figure 2k). Given that the collagen IV network allows the attachment of other proteins of the basal lamina, it creates a dense network that makes possible the upkeep of the pituitary gland. Then loss of its structure could have consequences on the rigidity of the tissue. In the same way, the fibers of laminin (basal lamina) organized in network in the normal tissue (Figure 2f) showed a strong decrease in the tumor tissue (Figure 2l). The loss of laminin observed is colocalized with

© 2021 The Authors. Advanced NanoBiomed Research published by Wiley-VCH GmbH

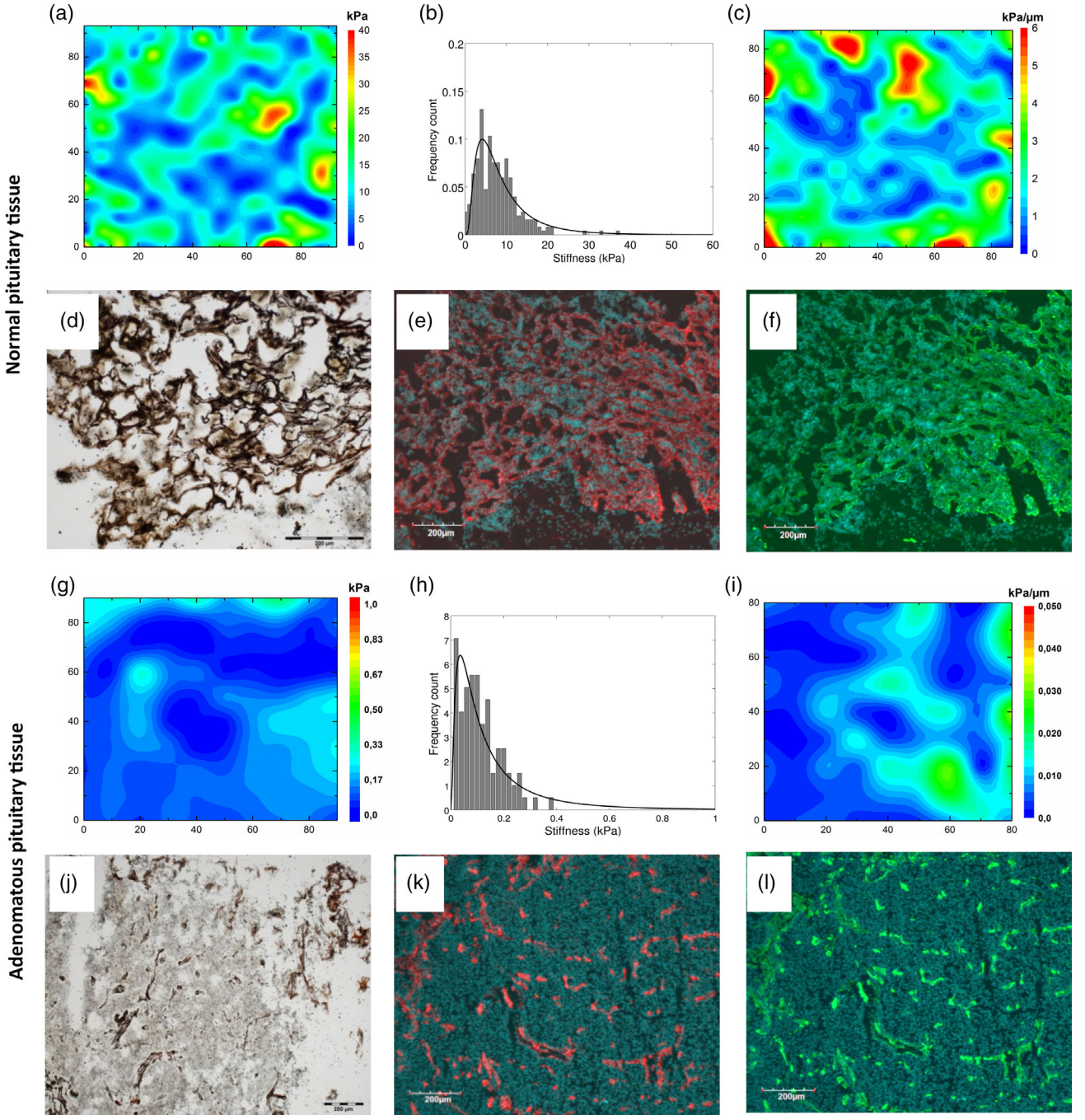

Figure 2. Comparison of the local micromechanical properties and ECM structure in pituitary gland tissues. a) Representative a specific AFM stiffness map (10 × 10 pixels) of the normal pituitary gland tissue and b) its corresponding stiffness distribution from the map. c) Map of the gradients of stiffness associated to (a). d) Post-AFM histology reveals normal pituitary gland tissue with reticulin, e) collagen IV (red), and f) laminin (green) labeling. g) Representative AFM stiffness map (10 × 10 pixels) of adenomatous pituitary gland tissue and h) the corresponding stiffness distribution from the map. i) Map of the gradients of stiffness associated to (g). j) Post-AFM histology reveals adenomatous pituitary gland tissue with reticulin labeling, k) collagen IV (red) and l) laminin (green) labeling. Bars in (d–f) and (j–l) 200 µm.

decreased expression of collagen IV. This can be explained by the fact that the laminin, glycoprotein of the basement membrane, attaches to the collagen IV network to complete the mesh structure.

Correlating with the dramatic decrease in the rigidity of adenomatous tissues, we thus observed a collapse of the basal lamina and consequently of the extracellular matrix which leads to a loss of the tissue architecture.

© 2021 The Authors. Advanced NanoBiomed Research published by Wiley-VCH GmbH

2.3. Micromechanical Softening is Observed Independent of the Pituitary Tumor Type

Pituitary adenomas comprise several tumor types, corresponding to different phenotypes with distinct hormonal disorders. We investigated whether the observed decrease in rigidity is applicable to the different classes of pituitary adenomas. To this end, we discriminated the rigidity test on the different classes of pituitary adenoma representative of the major types. Corticotropic adenoma secreting the ACTH that accounts for about 6% of all adenomas, growth hormone (GH) secreting somatotropic adenoma (13% of all adenomas), somatoprolactinic adenoma, secreting PRL and GH (PL/GH) (50% of the somatotropic adenomas), and gonadotropic adenomas, resulting from the gonadotropic cells secreting follicle-stimulating hormone (FSH) or luteinizing hormone (LH) (≈30% of the pituitary adenomas) were compared. Representative AFM stiffness maps showed an homogeneity in the rigidity of the adenomatous pituitary tissue with stiffness ranging from 0 to 0.5 kPa for all the pituitary adenoma types (**Figure 3**). This result was confirmed by the corresponding stiffness distributions obtained by concatenating all the measurements for each type of adenoma. Median values of the Young's moduli were ranging from 0.05 to 0.29 kPa depending on the tumor type (Figure 3f), but the variations of the median values were not significant. Welch's *t*-test provided *p*-values larger than 0.15 when comparing pairs of tumors and ANOVA Welch's *t*-test provided a *p*-value of 0.22. Overall, the loss of stiffness was observed on all types of pituitary adenoma with similar amplitude, regardless of the action of the tumor on the hypersecretion of hormones.

3. Discussion

Characterization of the mechanical properties of human tissues at subcellular resolution has recently emerged as tumor progression was shown to be sensitive to the cell-scaled mechanical properties of the tissue through integrin-mediated adhesion.[7,13,14] Magnetic resonance elastography (MRE) and ultrasound shear wave elastography (USWE) are the most used techniques to address tissue stiffness in clinics, as they are noninvasive and can be operated directly on the patient. MRE provides the maps of the rheological properties of the tissue that are averaged on volumes of few mm^3.[15] USWE is more resolved, with ability to discriminate few hundreds of μm.[4] Needle elastography has recently emerged with resolution down to 10–20 μm that makes it attainable to characterize the rheology of tissues at the cell scale.[16]

Ex vivo, IT-AFM allows scanning the mechanical properties of immersed samples down to nanoscale by indenting the tissue with a micron or nanometer-scaled probe.[14,17] Although it can currently not be carried out on the patient, the fact that it provides rheological measurements with enhanced resolution

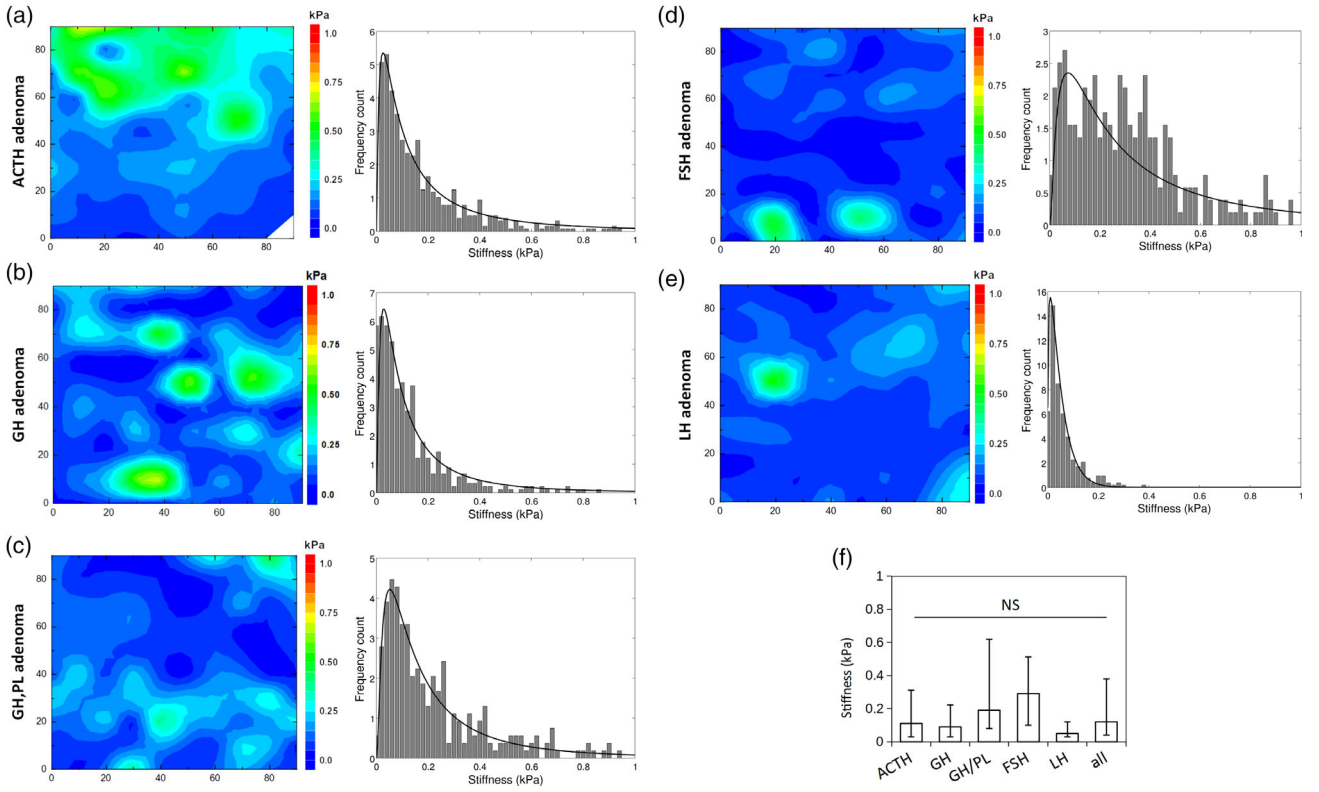

Figure 3. a–e) Representative AFM stiffness maps (10 × 10 pixels) of different pituitary adenoma types, with corresponding stiffness distributions: corticotropic adenoma secreting the ACTH, somatotropic adenoma-secreting GH, somatoprolactinic adenoma (GH/PL), and gonadotropic adenomas, derived from the secreting FSH or LH. f) Median stiffness for each type. Bars enclose 66% of the values. None of the stiffness medians significantly differs from each other (ANOVA Welch's *t*-test, $p = 0.22$).

© 2021 The Authors. Advanced NanoBiomed Research published by Wiley-VCH GmbH

may help to identify relevant mechanical markers appropriate for every tissue or cancer type. In this context, IT-AFM has already been used to characterize the stiffness of few tumor tissues. A majority of studies have reported increased stiffness following cancer. For instance, tissue stiffness was shown to be reinforced in tumor breast tissues.[2] Glioblastoma as well as compact tumor tissues from meningothelial meningioma (grade I WHO)[5] or medulloblastoma (grade IV WHO)[18] were also shown to be stiffer than healthy tissue. Differently, cirrhotic liver tissues demonstrated a softening in the presence of hepatocellular carcinoma.[19] All these mechanical mappings were carried out using nanoscale probes, thus reflecting the nanoscale variability of the mechanical properties of the tissues. From these data, it could be interpreted that the increase in the rigidity of the tissues from breast cancer, glioblastoma, meningothelial meningioma, or medulloblastoma comes from an increased content in stiff matrix proteins while reduced rigidity in cirrhotic liver tissues was attributed to the lower rigidity of tumor cells compared with normal cells.[5] Such conclusions were consistent with histological analysis and are also consistent with previous mechanical characterization obtained with MRE. IT-AFM also brought additional information compared with MRE on the cell-scaled gradients of rigidity that may influence cell fate. The study by Plodinec et al.,[2] for instance, evidenced more heterogeneous rigidity patterns at the periphery of the tumor compared with the center, associated with fibrotic tissues and cancer cell infiltration. From this observation, cell-scaled gradients of rigidity could emerge as an interesting marker as most migrating cell types were reported to migrate in response to stiffness gradients toward the stiffer regions.[20]

MRE or USWE provide centimeter scale maps of elasticity of the tissue. IT-AFM however is limited in the surface of tissues it can address due to acquisition times. As an order of magnitude, it takes 20 min to obtain a map of 100 pixels on a soft and sticky sample. The degradation of tissues then prevents from obtaining a representative collection of data with nanoscale resolution. In between IT-AFM mechanical mapping with nanometer resolution and MRE with millimeter resolution, the mechanical properties of the tissues averaged at the micrometer scale could be an alternative. Using micrometer-sized indenters, values of rigidity are then averaged on surfaces few μm^2. From the point of view of cell response, this micrometer scale is of equal interest as nanoscale. While it smooths the rigidity maps with giving micrometer-scaled averaged stiffness data, it provides information on stiffness on larger areas and still allows to discriminate cells from ECM when compared with histological staining.

Here, we explored the mechanical properties of pituitary adenoma using a micrometer-sized indenter, with 10 μm diameter. Then the values of rigidity we measured consisted of micrometer-averaged values on surfaces from 10 to 90 μm^2 (indentation depth from 0.5 to 3 μm). In this way, larger areas could be explored, 3–4 maps of 100 pixels on $90 \times 90\ \mu m^2$ area per sample could be acquired within a maximum of 2 h. Our main observation was that pituitary adenomatous tissues are on average a hundred times softer than healthy tissues (Figure 1). Tumor tissues that originate from different classes of adenoma were characterized. For all of them, we measured a similar drop of the stiffness (Figure 3). Consequently, we could not discriminate adenoma types on the basis of the mechanical measurement (Figure 3f). Compared with liver tissues which tumor tissues are also softer,[19] we predominantly attributed the lowering of the rigidity to the degradation of the matrix. As in the liver, softening of the cells may also contribute to the observed loss of rigidity, but the high rigidity of healthy tissues highlights the dominant role of the matrix. In the pituitary gland, the tissue architecture as well as its rigidity are closely linked to the content in reticulin, a protein of the ECM.[21] We observed that reticulin disorganizes from a dense network in healthy tissues to a much finer scaffold in adenoma (Figure 2d,j). In addition, the basal lamina which acts as a selective barrier between nonvascularized tissues and vascularized conjunctive tissue was also disrupted (Figure 2k–l). Basal lamina has an important function in regeneration after tissue damage, as it plays the role of framework on which the cells in regeneration can migrate. In this way, the original architecture of the tissues can be restored after lesion. The decrease in the expression of extracellular matrix proteins and glycoproteins in pituitary adenomas leads to an impossibility to restore the tissue during a lesion and may explain the cellular modification observed in the HE-stained sections. Stiffness maps also evidenced more uniform stiffness patterns than healthy tissues (Figure 2c,i). Combined with histological analysis, this suggests the absence of synthesis of a new basal lamina with abnormal composition which generally accompanies metastatic state. This observation is consistent with the fact that pituitary adenomas are benign tumors, and do not have metastasis in other tissues.

4. Conclusion

Here, we investigate the change in stiffness between healthy and adenoma tissues in the pituitary gland. The aim is to provide mechanical markers of the adenoma to help the surgical act. The challenge is of major importance especially in pituitary adenomas corticotroph whose morbidity and mortality is very important and which are often difficult to localize despite major progress in the field of imaging by MRI.[22] By measuring the micrometer-scaled averaged stiffness of normal and adenomatous tissues ex vivo with IT-AFM, we show that adenomatous tissues are a hundred times softer than healthy tissues and display more uniform stiffness patterns with gradients of stiffness reduced by a factor of a hundred. These results could serve future developments of in vivo diagnostic and surgery assistance devices dedicated to the pituitary gland, for instance the invasive needle elastography technique[16] or the development of noninvasive shear wave elastography probes.[23]

5. Experimental Section

Human Pituitary Tissue Samples: Pituitary tissue samples were obtained from the University Hospital Grenoble, Department of Neurosurgery. The human biopsies were residues from other research projects. As such, the French Public Health Code does not require compulsory formality, but recommend subjects information and consent. Informed written consent was obtained from the patients or their families. A total of eight pituitary tissue samples were collected from the operating room during trans-sphenoidal surgery of six patients and were immediately frozen at −80 °C. Pathologic diagnoses rendered based on routine histology, hormone immunostaining are shown in Table 1.

© 2021 The Authors. Advanced NanoBiomed Research published by Wiley-VCH GmbH

IT-AFM and Data Analysis: Frozen surgical specimen were cut in thick slices (150 µm in thickness) using a cryostat. The tissue slices were deposited on glass slides and stored at −20 °C. Just before the AFM experiment, the tissue slice was thawed at 26 °C for 30 min. As detailed in the study by Bouchonville et al.,[11] an incubation space was created by encircling the tissue section with a hydrophobic fat pen (Dako pen). Cautious washing was carried out with filtered PBS to remove residues of the hydrophobic barrier. The sample was then immediately immersed in filtered PBS and AFM measurements were carried out within the next 1–2 h at room temperature. Young's moduli of brain tissue samples were measured on a Nanowizard II AFM (JPK instruments, Berlin) in force mapping mode. MLCT D tipless cantilevers (Bruker, Santa Barbara) with a nominal spring constant of 0.03 N m^{-1} were chosen for their ability to address Young moduli between 0.1 and 100 kPa. A 10 µm polystyrene bead was glued to the cantilever to average the elastic properties on micrometer-sized area, i.e., averaging on the network composed of the cells and the extracellular matrix and not focusing on the nanoscale mechanical properties. Calibration of the cantilever was carried out before and after every sample to check the aging of the cantilever. For all experiments, indentation speed was set from 1 to 20 µm s^{-1} allowing us to check if the sample has any viscoelastic properties in this range.[11] Practically, we probed different locations of a specific tissue slice with distinct speeds and obtained statistically representative values of the rigidity for each indenting velocity (see Figure S1, Supporting Information). We ensured an indentation depth below 3 µm by adjusting the nominal force setpoint within 1–6 nN depending on the sample stiffness. The maps have a size of $90 \times 90\,\mu m^2$ and represent at least 100 force curves. Force–indentation curves were then fitted with the models described below in the range of indentation where the elastic deformation is linear as detailed in the studies by Bouchonville et al..[11,12] Smoothing was carried out on the maps of the Young's moduli to help the visualization of the rigidity texture using the interp2 function from Matlab with cubic interpolation and a meshgrid of 100 × 100 points.

AFM Data Post-treatment: Data were treated as explained in the study by Bouchonville et al..[12] First the part of the indentation curve that showed linear elastic response was delineated.[11] When several pieces of the curve showed a linear elastic behavior, the portion of the curve with forces ranging between 0.1 and 3 nN was preferred, in consistence with the amplitude of the cellular forces.[24] The selected part of the force–indentation curve was then fitted using Johnson–Kendall–Roberts (JKR) model for a spherical tip[25]

$$\delta = \frac{a_{JKR}^2}{R} - \frac{4}{3}\sqrt{\frac{a_{JKR} F_{adh}}{RK}} \quad (1)$$

$$a_{JKR} = \left(\frac{R}{K}\right)^{1/3} \left(\sqrt{F_{adh}} + \sqrt{F_n + F_{adh}}\right)^{2/3} \quad (2)$$

$$F_{adh} = \frac{3\pi}{2}\gamma R \quad (3)$$

with δ is the indentation relative to the surface of the sample, F_n is the indentation force, R is the radius of the spherical indenter. K is the renormalized elastic modulus that characterizes the linear elastic response of the sample. It relates to the elastic Young's modulus E and the Poisson's ratio ν of the material by the following formula: $K = 4E/3/(1-\nu^2)$. JKR model accounts for the possibility that the probe sticks to the sample: γ is the adhesive, interfacial energy of the indenter on the sample. In the absence of adhesion, $\gamma = 0$. From the fit, we obtain the elastic modulus of the sample, E, the adhesive energy γ between the spherical indenter and the sample, and the coordinate of the contact point of the indenter on the sample. Here, the Poisson ratio ν is assumed to be 0.45.[26] In principle, JKR model is valid for soft materials with large adhesion energy and probes with large radius of curvature compared with the indentation.[27] This corresponds to samples where the adhesion between the probe and the sample causes an indentation of the probe in the absence of external load that is large compared with the spatial range of the adhesion forces. These assumptions showed reasonable for tumor tissues, which Young's moduli span from about 50 Pa to few kPa. They are less relevant for the harder, normal tissue which Young's moduli span from few hundreds of Pa to few tens of kPa. Then another description of the adhesive interaction between the probe and the sample should be accounted, such as the Deraguin–Muller–Toporov (DMT) model.[28] However, both models led to very similar values of the fitting parameters in this case.[11] For this reason, we evaluated the elastic moduli of either tumor and normal tissues using JKR model.

Statistical Analysis: Eight specimens from six patients were analyzed, with surfaces ranging from 2 to 20 mm^2 (Table 1). Median values of the Young's moduli were obtained for each specimen, by analyzing about 200 to more than 900 curves (Table 1). The indentation points were organized in maps of $90 \times 90\,\mu m^2$. About 2–9 maps randomly distributed on the surface of the tissue section were acquired for each specimen. The fitted Young's moduli showed unimodal peaked distributions. We characterized the distribution on every specimen by calculating the median Young's modulus and the dispersion around the median. Dispersion around the median value was calculated from the 0.17 and 0.83 percentiles, which enclose 66% of the values. This interval was considered as a relevant indicator of the dispersion of the data for these non-normal distributions as it encloses a similar amount of data as the standard deviation in normal distributions.[29] Histograms of the distribution of the Young's moduli were fitted with log normal probability density function to guide the eye on the figures. ANOVA Welch's unequal variances t-test was carried out to analyze the statistical differences between the median values of the Young's moduli of all the maps of the adenoma types. A p-value of 0.22 was found, suggesting the absence of significant difference in between adenoma types. Welch's unequal variances t-test was then carried out to analyze the statistical differences between the median values of the Young's moduli of the pooled data of the tumor tissues and of the healthy tissues.

Histological Analysis: Frozen pituitary tissue samples were cut (20 µm in thickness) using a freezing microtome. For immunohistochemical (IHC) analysis, the following primary antibodies were used: anticollagen IV (1:500, Dakocytomation) and antilaminin (1/1000, Sigma Aldrich). Sections were incubated with these primary antibody solutions overnight at 4 °C. After washing, the secondary antibodies used were: 1:500 goat antimouse IgG Alexa 594 (1/500, Invitrogen) and goat antirabbit IgG Alexa 488 (1/500, Invitrogen) for collagen IV and laminin detection, respectively. All tissue sections were counterstained with 4′,6-diamidino-2-phenylindole (DAPI, Sigma Aldrich) and then mounted with FluorSave (Merck Millipore). Bound primary antibodies were visualized on a confocal microscope (Olympus).

HE staining and silver impregnation method for reticulin fibers were carried out on frozen sections mounted on glass slides using coloring kits (Kit Extempo, RAL Diagnostic and Silver impregnation, Diapth, respectively). HE-stained and reticulin slides were prepared to discriminate adenomatous tissue fragments from normal pituitary tissue.

Supporting Information

Supporting Information is available from the Wiley Online Library or from the author.

Acknowledgements

M.M. and N.B. contributed equally to this work. N.B. and A.N. acknowledge the support by ANR-12-JSVE05-0008. The authors thank the AFM platform of the Interdisciplinary Laboratory of Physics (LIPhy, Grenoble) for preparing the AFM tips.

Conflict of Interest

The authors declare no conflict of interest.

© 2021 The Authors. Advanced NanoBiomed Research published by Wiley-VCH GmbH

Data Availability Statement

Data available on request from the authors.

Keywords

indentation-type atomic force microscopy, mechanobiology of tumor tissues, pituitary adenomas, stiffnesses

Received: November 16, 2020
Revised: April 20, 2021
Published online: July 3, 2021

[1] E. J. Song, Y.-M. Sohn, M. Seo, *Br. J. Radiol.* **2018**, *91*, 20170830.
[2] M. Plodinec, M. Loparic, C. A. Monnier, E. C. Obermann, R. Zanetti-Dallenbach, P. Oertle, J. T. Hyotyla, U. Aebi, M. Bentires-Alj, R. Y. H. Lim, C.-A. Schoenenberger, *Nat. Nanotechnol.* **2012**, *7*, 757.
[3] E. J. Koay, Y. Lee, V. Cristini, J. S. Lowengrub, Y. Kang, F. A. S. Lucas, B. P. Hobbs, R. Ye, D. Elganainy, M. Almahariq, A. M. Amer, D. Chatterjee, H. Yan, P. C. Park, M. V. Rios Perez, D. Li, N. Garg, K. A. Reiss, S. Yu, A. Chauhan, M. Zaid, N. Nikzad, R. A. Wolff, M. Javle, G. R. Varadhachary, R. T. Shroff, P. Das, J. E. Lee, M. Ferrari, A. Maitra, et al., *Clin. Cancer Res.* **2018**, *24*, 5883.
[4] D. Chauvet, M. Imbault, L. Capelle, C. Demene, M. Mossad, C. Karachi, A.-L. Boch, J.-L. Gennisson, M. Tanter, *Ultraschall Med.* **2016**, *37*, 584.
[5] G. Ciasca, T. E. Sassun, E. Minelli, M. Antonelli, M. Papi, A. Santoro, F. Giangaspero, R. Delfini, M. De Spirito, *Nanoscale* **2016**, *8*, 19629.
[6] C. Rianna, P. Kumar, M. Radmacher, *Semin. Cell Dev. Biol.* **2018**, *73*, 107.
[7] F. Kai, A. P. Drain, V. M. Weaver, *Dev. Cell* **2019**, *49*, 332.
[8] B. W. Scheithauer, *Pathol. Annu.* **1984**, *19 Pt 1*, 317.
[9] M. G. Lake, L. S. Krook, S. V. Cruz, *Am. Fam. Physician* **2013**, *88*, 319.
[10] N. Fukuhara, N. Inoshita, M. Yamaguchi-Okada, K. Tatsushima, A. Takeshita, J. Ito, Y. Takeuchi, S. Yamada, H. Nishioka, *Endocr. J.* **2019**, *66*, 259.
[11] N. Bouchonville, M. Meyer, C. Gaude, E. Gay, D. Ratel, A. Nicolas, *Soft Matter* **2016**, *12*, 6232.
[12] N. Bouchonville, A. Nicolas, *Methods Mol. Biol.* **2019**, *1886*, 281.
[13] J. K. Mouw, Y. Yui, L. Damiano, R. O. Bainer, J. N. Lakins, I. Acerbi, G. Ou, A. C. Wijekoon, K. R. Levental, P. M. Gilbert, E. S. Hwang, Y.-Y. Chen, V. M. Weaver, *Nat. Med.* **2014**, *20*, 360.
[14] M. Krieg, G. Fläschner, D. Alsteens, B. M. Gaub, W. H. Roos, G. J. Wuite, H. E. Gaub, C. Gerber, Y. F. Dufrêne, D. J. Müller, *Nat. Rev. Phys.* **2019**, *1*, 41.
[15] M. C. Murphy, J. Huston, R. L. Ehman, *Neuroimage* **2019**, *187*, 176.
[16] D. Wickramaratne, P. Wilkinson, J. Rao, N. Ragavendra, S. Sharma, J. K. Gimzewski, *J. Biomech.* **2015**, *48*, 81.
[17] M. Li, D. Dang, L. Liu, N. Xi, Y. Wang, *IEEE Trans. Nanobiosci.* **2017**, *16*, 523.
[18] H. Abramczyk, A. Imiela, *Spectrochim. Acta. A. Mol. Biomol. Spectrosc.* **2017**, *188*, 8.
[19] M. Tian, Y. Li, W. Liu, L. Jin, X. Jiang, X. Wang, Z. Ding, Y. Peng, J. Zhou, J. Fan, Y. Cao, W. Wang, Y. Shi, *Nanoscale* **2015**, *7*, 12998.
[20] M. J. Oudin, V. M. Weaver, *Cold Spring Harbor Symp. Quant. Biol.* **2016**, *81*, 189.
[21] S. Noh, S. H. Kim, N. H. Cho, S. H. Kim, *Endocr. Pathol.* **2015**, *26*, 178.
[22] R. S. Dhillon, J. A. King, T. Goldschlager, Y. Y. Wang, *ANZ J. Surg.* **2018**, *88*, 460.
[23] A. V. Polat, M. Ozturk, A. K. Polat, U. Karabacak, T. Bekci, N. Murat, *J. Ultrasound Med.* **2020**, *39*, 795.
[24] U. Schwarz, *Soft Matter* **2007**, *3*, 263.
[25] K. L. Johnson, K. Kendall, A. D. Roberts *Proc. R. Soc. Lon. Ser. A* **1971**, *324*, 301.
[26] G. Soza, R. Grosso, C. Nimsky, P. Hastreiter, R. Fahlbusch, G. Greiner, *Int. J. Med. Rob. Comput. Assisted Surg.* **2005**, *1*, 87.
[27] D. Maugis, *J. Colloid Interf. Sci.* **1992**, *150*, 243.
[28] B. Derjaguin, V. Muller, Y. Toporov, *J. Colloid Interf. Sci.* **1975**, *53*, 314.
[29] E. Limpert, W. A. Stahel, *PLoS One* **2011**, *6*, e21403.

© 2021 The Authors. Advanced NanoBiomed Research published by Wiley-VCH GmbH